Atmos. Chem. Phys. Discuss., 15, 30757–30791, 2015
www.atmos-chem-phys-discuss.net/15/30757/2015/
doi:10.5194/acpd-15-30757-2015

Atmospheric Chemistry and Physics Discussions

Properties of cloud condensation nuclei (CCN) in the trade wind marine boundary layer of the Eastern Caribbean Sea

T. B. Kristensen[1], T. Müller[1], K. Kandler[2], N. Benker[2], M. Hartmann[2], J. M. Prospero[3], A. Wiedensohler[1], and F. Stratmann[1]

[1]Leibniz Institute for Tropospheric Research, 04318 Leipzig, Germany
[2]Environmental Mineralogy, Institute of Applied Geosciences, Technische Universität Darmstadt, 64287 Darmstadt, Germany
[3]Rosenstiel School of Marine and Atmospheric Science, University of Miami, Miami, FL, USA

Received: 5 October 2015 – Accepted: 15 October 2015 – Published: 5 November 2015

Correspondence to: T. B. Kristensen (kristensen@tropos.de)

Published by Copernicus Publications on behalf of the European Geosciences Union.

Abstract

Cloud optical properties in the trade winds over the Eastern Caribbean Sea have been shown to be sensitive to cloud condensation nuclei (CCN) concentrations. The objective of the current study was to investigate the CCN properties in the marine boundary layer (MBL) in the Eastern Caribbean, in order to assess the respective roles of organic species, long-range transported mineral dust, and sea salt particles.

Measurements were carried out in June–July 2013, on the East Coast of Barbados and included CCN number concentrations, particle number size distributions, as well as off-line analysis of sampled particulate matter (PM) and sampled accumulation mode particles for an investigation of composition and mixing state with transmission electron microscopy (TEM) in combination with energy-dispersive X-ray spectroscopy (EDX).

During most of the campaign, significant mass concentrations of long-range transported mineral dust was present in the PM, and influence from local island sources can be ruled out. The CCN and particle number concentrations were similar to what can be expected in pristine marine environments. The hygroscopicity parameter κ was inferred, and values in the range 0.2–0.5 were found during most of the campaign, with similar values for the Aitken and the accumulation mode. The accumulation mode particles studied with TEM were dominated by non-refractory material, and concentrations of mineral dust, sea salt, and soot were too small to influence the CCN properties. It is highly likely that the CCN were dominated by a mixture of sulphate species and organic compounds.

1 Introduction

Clouds play an important role with respect to the radiation budget and thus climate on Earth. The concentration of cloud condensation nuclei (CCN) in the atmosphere influences the optical and physical properties of clouds (Andreae and Rosenfeld, 2008). Significant uncertainties are related to the radiative forcing of aerosol–cloud interac-

ACPD
15, 30757–30791, 2015

tions in the climate system (IPCC, 2013). Global climate is in particular sensitive to aerosol–cloud interactions over the oceans due to the large surface of the oceans and the significant difference in albedo between clouds and the open ocean. There are significant climate-relevant uncertainties related to the CCN budget in the marine environment (Pierce and Adams, 2006), and in general it is very challenging to incorporate marine boundary layer (MBL) clouds correctly in climate models (Bony and Dufresne, 2005).

Submicrometer aerosol particles in the pristine North Atlantic marine environment are comprised of sea salt as well as sulfate and organic species dominating during periods with high marine biological activity (O'Dowd et al., 2004). With typically relatively low background aerosol particle number concentrations in the pristine MBL the CCN number concentrations may be perturbed significantly e.g. due to long range transport. Mineral dust particles from Northern Africa are transported by the trade winds across the Atlantic Ocean particularly during the summer season in the Northern Hemisphere (Prospero and Lamb, 2003). Twohy et al. (2009) reported that a large fraction (79 %) of cloud droplet residual particles were comprised of crustal material in the Eastern Northern Atlantic. Jung et al. (2013) reported a hygroscopicity parameter, κ value of 0.02–0.03 for the accumulation mode particles at different altitudes including the MBL, east of Barbados during a pronounced mineral dust episode. Such low κ values close to 0.01 as for pure dust (Garimella et al., 2014; Petters and Kreidenweis, 2007) are indicative of an accumulation mode dominated by dust with only minor amounts of hygroscopic particulate matter (PM) present. Hence, mineral dust particles may play an important role as CCN under certain conditions over the North Atlantic.

Continuous measurements related to aerosol particle properties have been carried out on the east coast of Barbados since the mid 1960s (Prospero and Lamb, 2003). Upwind from the east coast of Barbados there is typically ~ 4000 km of Atlantic Ocean due to the dominating easterly trade winds. Hence, aerosol particles in the Eastern Caribbean are typically of marine origin or are transported over long distances across the Atlantic Ocean. Savoie et al. (1989, 2002) investigated the composition of bulk PM

ACPD
15, 30757–30791, 2015

sampled on the East coast of Barbados from the periods 1984–1987 and 1988–1991 respectively. Savoie et al. (1989) reported high correlations between the concentrations of non-sea-salt (nss) NO_3^-, nss SO_4^{2-}, and mineral dust which they ascribed to similar transport pathways of the mineral dust and the investigated water soluble nss inorganic species. Furthermore, they reported a minimum in the NO_3^- to SO_4^{2-} ratio in summer and suggested that Europe was likely to be the source region of those species during the summer season. Savoie et al. (2002) reported that biogenic marine nss SO_4^{2-} reaches maximum concentrations around May–June and comprises about 50 % of total nss SO_4^{2-} on a yearly average. Li-Jones and Prospero (1998) sampled size segregated PM at the same site during April 1994, and they found that nss SO_4^{2-} dominated the PM with aerodynamic diameters smaller than 0.6 µm, while the supermicron PM primarily was comprised of mineral dust, sea salt, nss NO_3^-, and smaller amounts of nss SO_4^{2-}.

In addition to dust and water soluble salts, aerosol particles relevant as CCN over the Caribbean Sea may also contain organic compounds. A number of studies with focus on organic PM have been conducted primarily on or in the vicinity of Puerto Rico, and they are reviewed and summarised by Allan et al. (2008). In short, past studies indicate that there is a significant fraction of organic matter in PM with diameters < 0.6 µm (Novakov et al., 1997), the organic species are hygroscopic (Maria et al., 2002) and efficient as CCN (Novakov and Penner, 1993; Novakov et al., 1997). Mayol-Bracero et al. (2001) attributed significant amounts of the organic matter to natural oceanic sources. In contrast to most previous studies Allan et al. (2008) reported low concentrations of organic matter mostly attributed to local anthropogenic emissions. The optical properties of trade wind cumuli clouds over the Eastern Caribbean Sea are susceptible to increased levels of CCN and direct evidence for the Twomey effect has clearly been observed (Werner et al., 2014). The strong insolation at low latitudes and the remote location makes Barbados an ideal location for studying climate effects of long range transported CCN in the marine environment.

Only few studies of CCN properties have previously been carried out over the Caribbean Sea, and based on the limited and very different results reported, it is not

ACPD
15, 30757–30791, 2015

evident what the dominant CCN properties are in that region. The objective of the current study is to investigate to what extent organic species, nss inorganic species, sea salt, and long-range transported Saharan mineral dust may influence the CCN properties in that region. The CCN activity was inferred from CCN concentrations in conjunction with particle number size distribution measurements. Particles in the dominant CCN size range were also investigated with transmission electron microscopy (TEM) combined with energy-dispersive X-ray spectroscopy (EDX), in order to identify refractory PM such as sea salt and mineral dust, and for estimation of the volume fractions of different types of PM. The present study was carried out on Barbados as part of the Saharan Aerosol Long-range Transport and Aerosol-Cloud-Interaction Experiment (SALTRACE) campaign during June–July 2013.

2 Theory

The equilibrium saturation ratio of water vapour over an aqueous solution droplet can be described by the the Köhler equation. Petters and Kreidenweis (2007) introduced the hygroscopicity parameter κ and formulated the Köhler equation as:

$$\frac{\mathrm{SS}}{[100\,\%]} = \frac{D_\mathrm{d}^3 - D_\mathrm{p}^3}{D_\mathrm{d}^3 - D_\mathrm{p}^3(1-\kappa)} \exp\left(\frac{4\sigma M_\mathrm{w}}{\mathrm{R}T\rho_\mathrm{w} D_\mathrm{d}}\right) - 1 \quad (1)$$

where SS is the supersaturation in %, M_w is the molar mass of water, ρ_w is the density of water, σ is the surface tension, $R = 8.314\,\mathrm{J\,(K\,mol)^{-1}}$ is the universal gas constant, T is the absolute temperature, D_p and D_d are the dry particle and droplet diameters respectively. The hygroscopicity parameter κ ranges from about 0 for nonhygroscopic components to ~ 1.4 for very hygroscopic species (Petters and Kreidenweis, 2007).

Based on the Zdanovskii, Stokes, and Robinson (ZSR) assumption (Petters and Kreidenweis, 2007) the κ value of mixed particles can be estimated by a volume weighted

ACPD
15, 30757–30791, 2015

addition of the κ values of the pure compounds:

$$\kappa_{\text{add}} = \sum \varepsilon_i \kappa_i \quad (2)$$

where κ_i is the κ value of the species i and ε_i is the volume fraction of species i in the dry particles.

3 Experimental

The main part of the SALTRACE campaign was carried out from mid-June to mid-July, 2013 and involved a number of different atmospheric measurements mostly based on Barbados. The aim of the campaign was to investigate properties of Saharan mineral dust transported across the North Atlantic to the Caribbean Sea. The campaign included airborne measurements west of Africa as well as in the vicinity of Barbados. A pronounced Saharan mineral dust layer was present at altitudes of 2-4 km over Barbados almost during the entire campaign (Groß et al., 2015). The ground based aerosol measurements included in the present study were carried out at Ragged Point (13°09′54″ N, 59°25′56″ W) on the East Coast of Barbados. Studies of long range transported aerosol particles have been carried out on the east coast of Barbados since the mid-1960s and at Ragged Point since the early 1970s (Prospero and Lamb, 2003).

For the in-situ measurements, the ambient aerosol was sampled through a PM_{10} inlet located ~ 50 m a.s.l. at the top of a 17 m high tower located on the edge of a 30 m high rocky promontory adjacent to the ocean. The flow rate was 16 L min^{-1} inside a 3/4 inch stainless steel tube leading down to the ground level where different instruments were connected. Among the instruments were an Aerodynamic Particle Sizer (APS-3321, TSI), a mobility particle size spectrometer (MPSS, TROPOS-REF-3) (Wiedensohler et al., 2012) measuring the particle number size distributions in parallel with a condensation particle counter (CPC-3010, TSI) determining the total particle number

ACPD
15, 30757–30791, 2015

concentration, and a CCN counter (CCNC) from Droplet Measurement Technologies, USA (Roberts and Nenes, 2005), measuring the total number concentration of CCN at different supersaturations in the range from 0.1 to 0.7 %. These instruments (except for the APS) were all located inside an air conditioned container with the temperature kept constant at ~ 25 °C. The sample aerosol was dried to $\lesssim$ 40 % with a Nafion® dryer inside the container before being investigated. Particle number size distributions were obtained for every ~ 14 min. The supersaturation settings of the CCNC changed every 10–15 min – in order to allow for the supersaturations to stabilise and still ensure a significant overlap in time with a measured particle number size distribution.

Samples for off-line analysis were collected at the top of the tower. A high volume sampler was used to sample total PM on 20 cm × 25 cm Whatman 41 filters with a flow rate of ~ 1 m^3 for analysis of the mineral dust concentration. A daily resolution was obtained and sampling typically started around 10:00 UTC. In order to minimize impacts from local sources sampling was controlled by a wind sensor and only carried out when the local wind direction was in the range 335° through North to 130°, and the wind speed exceeded 1 m s^{-1}. A quarter of each filter was rinsed with pure water and placed in a muffle furnace for 14 h at 500 °C. The mass of mineral dust was estimated from multiplying the mass of the remaining ash by 1.3. More details about the sampling sector and the procedure for inferring the mineral dust concentration are available in the literature (Prospero et al., 2005; Trapp et al., 2010).

Samples for TEM analysis were also collected at the top of the tower with a miniature cascade impactor (Kandler et al., 2007) on TEM Ni-grids coated with a formvar carbon film (FCF200F1-Ni, Science Services, Munich, Germany). The nominal cut-off aerodynamic diameters for the stages analysed in the present work are 530 nm (upper) and 90 nm (lower) during the period from 15 to 21 June 2015, and 330 nm (upper) and 90 nm (lower) during the period from 22 June to 15 July. Sampling was performed under ambient conditions with the impactor inlet oriented pseudo-isoaxially. While the flow conditions were considerably sub-isokinetic, for the regarded particles diameter

ACPD
15, 30757–30791, 2015

range from 50 to 300 nm an aspiration bias is negligible. The samples were stored in a drying cabinet (silica gel) at ambient temperature.

Meteorological measurements were carried out at the top of the tower and included measurements of wind speed, wind direction, precipitation, temperature and humidity.

4 Data analysis

4.1 Cloud condensation nuclei and particle number size distributions

For an estimation of the CCN activity, the average CCN number concentration was compared to the simultaneously measured particle number size distribution in order to estimate a critical diameter (D_c) above which all particles activate into cloud droplets for a given supersaturation. The critical mobility diameter is inferred by integrating the particle number size distribution from the largest particle diameter and downwards until a particle number concentration equal to the CCN concentration is obtained (e.g. Jurányi et al., 2010). This approach relies on the fact that the dry particle size is a very important parameter for whether a particle will activate into a cloud droplet (as given in Eq. 1).

In order to obtain a best estimate of and the error on the critical diameter, the integrations were carried out for 10 000 Monte Carlo simulations, for which the errors on the CCN number concentration and the MPSS number concentrations in different size channels were taken into account. The relative random error on the CCN number concentration corresponding to one standard deviation was assumed to be represented by the inverse of the square root of the total CCN counts during a given time interval. The relative random error on the MPSS derived particle number concentration in a given size channel corresponding to one standard deviation was assumed to be represented by 5 %. It was found to be a reasonable estimate of the random error from intercomparisons of neighbouring MPSS particle number size distributions during time periods where the total number concentration changed negligibly. The calibration of the

ACPD
15, 30757–30791, 2015

CCNC in the laboratory prior to and after the campaign clearly showed some systematic losses of ultrafine particles increasing linearly with decreasing particle diameters below ~ 80 nm. This effect is likely to be due to diffusional losses inside the CCNC (Rose et al., 2008). These losses were assumed to be the same in the field as in the laboratory, and this effect was accounted for in the data analysis when inferring the critical diameter.

The inferred probability density functions of the critical diameters were generally found to be well represented by Gaussian distributions.

Based on the supersaturation and the inferred critical diameter the hygroscopicity parameter κ was calculated (Petters and Kreidenweis, 2007). The error on the CCNC supersaturation is estimated based on the variation among numerous calibrations carried out in the laboratories at the Leibniz Institute for Tropospheric Research (Tropos). For SS $\geq$ 0.2 % the variation in the supersaturation appeared to be represented very well by a Gaussian distribution with a standard deviation of 0.037 % in relative terms. For SS $<$ 0.2 % an absolute value of 0.03 % SS represented one standard deviation. Rose et al. (2008) reported lower variations in the SS under controlled laboratory conditions (~ 1 %) and larger relative errors while operating in the field (~ 5 %) mainly due to temperature variations.

The probability density functions of the critical diameter and the supersaturation as described above were used as independent input for the calculation of the probability density functions of κ. The temperature at activation was estimated to be $0.5 \cdot (T_1 + T_2)$ where T_1 and T_2 are the temperatures at the top and at the midpoint of the CCNC column wall respectively. The temperature enters directly in Eq. (1) and it also enters indirectly through an influence on σ and ρ_w in Eq. (1). A surface tension of pure water was assumed in the κ calculations and a parameterisation of $\sigma(T)$ was obtained from results reported in the literature (Cini et al., 1972).

There were some systematic problems with the temperature setting at the bottom of the CCNC column wall (T_3) being too low (SS = 0.074 %) for the SS = 0.1 % setting during the last weeks of the campaign. It was possible to correct for this error on the

ACPD
15, 30757–30791, 2015

SS in combination with the size distributions due to a systematic alternation between correct and off-set T_3 settings, and it has been taken into account in all the results shown in the present study.

A very good agreement was found between the used MPSS and a reference MPSS before and after the campaign (Wiedensohler et al., 2012). The MPSS sizing was validated in the field at the beginning and at the end of the campaign with mono-disperse polystyrene latex spheres (PSL) with a diameter of 203 nm.

4.2 Transmission electron microscopy (TEM)

The TEM analysis was carried out in order to provide information about the chemical composition of the aerosol particles. TEM grid samples were analysed with a Philips CM 20 (FEI, Eindhoven, the Netherlands) operated at 200 kV accelerating voltage and a LaB_6 gun. The images were recorded with a CCD camera (KeenView G2, Olympus Soft Imaging Solutions GmbH, Münster, Germany) mounted at the bottom of the electron microscope. The Transmission electron microscope is equipped with an energy-dispersive X-ray microanalysis with a Silicon Drift detector (X-Max 80 mm^2, Oxford, Oxfordshire, UK). Images were acquired with a resolution of 1.32 pixels per nm. As during particle analysis, the volatile material of the particle evaporates and the refractory fraction remains, images were recorded at the beginning of the electron bombardment and after no more visible change in particle structure occurred. An exact temperature under this electron bombardment can not be determined. However, the temperature conditions can be considered to be similar for all measurements, as identical instrument settings were used. From a chemical analysis it becomes obvious that nitrate and sulfate evaporated, while sodium chloride, all mineral dust components and soot remain stable (Kandler et al., 2011). From the decomposition behavior and the absence of sodium chloride melting, we can conclude that the temperature is between 200 and 800 °C, most likely higher than 300 °C (Kiyoura and Urano, 1970; Lide, 2009). Semi-automatic image analysis (determination of the particle projected area and the projected-area-equivalent diameter (PAED)) was performed with the ImageJ software

ACPD
15, 30757–30791, 2015

1.47c (Rasband, 2015). As the brightness of the images is uneven, instead of an automatic brightness-based segmentation procedure a manual thresholding combined with additional manual particle outlining was required. The volume fraction of refractory material inside each particle was estimated as the ratio of the projected area after evaporation to the projected area before evaporation, raised to the power of 1.5.

5 Results

5.1 Local airmass characteristics

Locally measured wind speed, wind direction, relative humidity (RH) and precipitation are shown in Fig. 1 for the time period from 14 June to 15 July, 2013, corresponding to the day of year (DOY) range from 165 to 196. All times presented in this section are in UTC (corresponding to LT+4 h). The wind speed shown in the top-panel of Fig. 1 ranged from ~ 2 to $\sim 15\,m\,s^{-1}$ with an average value of $8.8\,m\,s^{-1}$. The wind direction was dominated by easterly winds (Fig. 1-mid-panel). With wind directions in the range from 335° through North to 130° only the open ocean is upwind from the field station. The 130° wind direction level is indicated in the mid-panel of Fig. 1, and time periods where the wind direction is in the range from 130 to 360° are indicated with a grey background. For > 95 % of the time the wind direction was in the range from 0 to 130°. Only one time during the campaign a small vessel was noticed within eyesight of the measurement station. This indicates that local and land-based emissions are unlikely to influence our observations during most of the campaign. The local ambient temperature was on average 26.0 °C with diurnal variations typically being < 1 °C. The ambient RH ranged from ~ 65 to ~ 85 % during most of the campaign (Fig. 1 – lower panel). Elevated levels of RH were typically associated with time periods with precipitation – which are indicated with blue in the lower panel in Fig. 1. Intense showers lasting for short time periods (often < 1 h) occurred frequently during the campaign.

ACPD
15, 30757–30791, 2015

5.2 Particle number size distributions, CCN concentrations and CCN activity

The measured particle number size distributions (not corrected for losses in sampling lines and detection efficiency) are shown in Fig. 2. In the top panel of Fig. 2 the time series of the particle number size distributions are shown, and in the lower panel the median particle number size distribution and the median volume particle size distribution over the whole campaign are shown. The size range of mobility particle diameters from 0.01 to 0.8 µm is covered by MPSS data merged with APS measurements for volume equivalent diameters above 0.8 µm. The gaps in the data in the top panel are due to lack of measurements.

During most of the campaign the typical marine particle number size distribution with two submicrometer modes can be observed: an Aitken mode with a maximum close to 50 nm and an accumulation mode with a maximum close to 180 nm (Heintzenberg et al., 2004). A Hoppel minimum is typically observed around a mobility diameter of 80 nm. The average critical diameters (more details given below) are also indicated in the figure and it is evident that for the lowest supersaturations (0.1–0.3 %) information about the accumulation mode is typically provided, while information about the Aitken mode is provided for higher supersaturations. It is also clear from the median particle number size distribution that very low number concentrations are present in the supermicrometer range. The median particle volume size distribution inferred from assuming spherical particles is shown in the lower panel to the right in Fig. 2. The volume size distribution is dominated by particles larger than ~ 0.5 µm, with a maximum generally reached at 2 µm followed by an abrupt decrease for larger particle diameters. The abrupt decrease is most likely due to losses of coarse mode particles in the sampling lines. The correction for losses of coarse particles in the sampling lines is uncertain, and have thus not been carried out. The total particle number concentration is typically in the range from 200–400 cm^{-3}, with a few exceptions often associated with time periods, where influence from local land-based particle sources cannot be ruled out. Hence, the total marine background particle number concentration observed is in the

ACPD
15, 30757–30791, 2015

lower end of the typical concentrations of 300–600 cm^{-3} found in the MBL (O'Dowd and de Leeuw, 2007).

The measured number concentrations of CCN vs. time are shown in the upper panel of Fig. 3. The CCN number concentrations stay rather constant throughout the campaign with a few exceptions with remarkably reduced concentrations and one episode with elevated concentrations around the DOY = 185.5 (4 July). The time periods with low CCN concentrations are associated with higher RH than average and also more precipitation than average as can be seen from the lower panel of Fig. 1. The median CCN number concentrations are included in Table 1 and range from $\sim 80\,cm^{-3}$ for an SS = 0.1 % to $\sim 240\,cm^{-3}$ for an SS = 0.7 %. Those CCN number concentrations are comparable to what has been observed over the western North Pacific (Mochida et al., 2011), and over the North Atlantic for clean marine conditions (Reade et al., 2006), but often higher concentrations of CCN are observed in the MBL (Good et al., 2010; Jefferson, 2010; Sorooshian et al., 2009).

The critical diameters inferred as described above in Sect. 4.1 are shown in the mid-panel of Fig. 3. The calculated random errors are not shown in the figure. For the SS = 0.1 % the random errors corresponding to one standard deviation are in the range from ~ 2 to ~ 10 nm, while for higher SS the similar errors are in the range from ~ 1 to ~ 5 nm with decreasing average values with increasing SS. The average random errors on the critical diameter (δD_c) are included in Table 1. The critical diameters are slightly lower during the first days of measurements, but they appear to stay fairly constant throughout most of the campaign. For an SS = 0.1 % the D_c stays above 100 nm, and for an SS = 0.2 % the D_c is typically slightly above the Hoppel minimum so those data provide information about the accumulation mode CCN activity, while for higher SS information about the Aitken mode CCN activity is obtained.

The calculated κ values vs. time are shown in the lower panel of Fig. 3. The κ values are quite similar for the different supersaturations and thus also similar for the accumulation mode and the Aitken mode during the entire campaign. The probability density functions of the inferred κ values were found to be very well approximated by

ACPD
15, 30757–30791, 2015

a Gaussian distribution in the range of ±1 standard deviation relative to the median κ value. The random errors on κ representing one standard deviation ($\delta\kappa$) were on average 0.05 and increasing slightly with the supersaturation. The average $\delta\kappa$ values are included in Table 1. During the first day of measurements (DOY = 165, 14 June), the κ values are typically around or above ∼ 0.6. In the time period from 168.0–173.0 DOY (17–21 June) most of the κ values are typically in the range from 0.3 to 0.5. During the last 22 days of measurements (22 June to 14 July) most of the κ values are found in the range from 0.2 to 0.4.

The higher κ values above 0.6 during the first day is likely to be at least partly due to sea salt since most other species present in ambient aerosol have κ values close to or below 0.6 (Petters and Kreidenweis, 2007; Petters et al., 2009). The observations of elevated κ values coincide with the highest local wind speeds (∼ 14 m s^{-1}) observed during the campaign. It fits with the expectation of the flux of sea spray particles depending highly on the wind speed (Monahan and Muircheartaigh, 1980; O'Dowd and de Leeuw, 2007).

The κ values inferred here are lower than the values of 0.6 ± 0.2 for Puerto Rico and 0.87 ± 0.24 for Antigua reported by Pringle et al. (2010) based on the measurements presented by Allan et al. (2008) and Hudson (2007) respectively. The κ values from the first day of our measurements is comparable to the other literature values for the Carribean. It is worth noting that the previous measurements were carried out in December and January respectively and it is likely that the chemical PM composition changes with the seasons (Savoie et al., 1989).

5.3 Mineral dust concentration

The daily total mass concentrations of mineral dust during the campaign are depicted as bars in Fig. 4 together with the estimated total mass concentration (PM_{est}) based on the integrated particle volume size distributions for diameters larger than 0.5 µm. Both of the depicted time series only represent time periods when the local wind direction indicated no influence from local land based sources as described above. Most of the

ACPD
15, 30757–30791, 2015

dust concentrations are based on sampling for ∼ 24 h, and all the shown dust concentrations are based on > 12 h of sampling – depending on the local wind direction. The average mineral dust concentration during the campaign is ∼ 19 µg m^{-3}, with noticeable variations on a daily scale. The maximum of the daily mineral dust concentration of ∼ 80 µg m^{-3} was observed for 11–12 July (DOY = 192.4–193.4), which is a high concentration for this site. Only occasionally the daily average mineral dust mass concentration exceeds 100 µg m^{-3} (Savoie and Prospero, 1977; Savoie et al., 1987; Jung et al., 2013). A strong yearly cycle of the mineral dust concentration is present in this region with maximum concentrations in June–July (Prospero and Lamb, 2003), and significant (occasionally high) concentrations of dust were indeed present in the MBL during almost the entire campaign.

The mass concentrations estimated from the integrated volume size distributions shown in Fig. 4 are based on the assumptions of spherical particles and a particle density of 2.6 g cm^{-3} as for mineral dust (Bergametti and Forêt, 2014). The estimated total mass concentrations are likely to be biased low due to losses in the sampling tube and inlet, but it may also result in higher concentrations than for pure dust due to non-dust particles such as e.g. sea salt. However, there is a very significant linear correlation between the two data series depicted in Fig. 4 with a correlation coefficient of $r = 0.85$ for the 30 days where data was available. From Fig. 4 it can also be seen that the magnitude of the two mass concentrations are comparable typically within a factor of 2. These observations indicate that the coarse particles dominating the volume size distribution (Fig. 2) primarily are comprised of mineral dust. Hence, the estimated total mass concentrations inferred from the measured particle number size distributions can be used as a proxy of the mineral dust concentration with a higher time resolution. Thus, it can be determined whether high or low dust concentrations could be expected e.g. during the relatively short time periods used for collecting samples for investigation with transmission electron microscopy.

ACPD
15, 30757–30791, 2015

5.4 Transmission electron microscopy (TEM)

Samples were collected on eight different days, where the mineral mass dust concentration was close to or above the average for seven out of the eight samples, based on the data presented in Fig. 4. Details about the sampling times of the samples are provided in Table 2. By use of TEM in combination with EDX information about the respective volume fractions of non-refractory and refractory particulate matter and information about the chemical composition of the latter was obtained. Thus, the TEM data provides a strong basis for interpretation of the CCN properties presented above. Some examples of images of the studied particles are shown in Fig. 5. The particle shown in Fig. 5I.a is non-refractory and on timescales of seconds it evaporates. As can be observed in Fig. 5I.b, only an indication of a thin layer remains on the spot were the particle used to be. Similar types of particles have also been observed on Cape Verde with the same technique, and the remaining thin layer was suggested to be comprised of refractory organic compounds (Kandler et al., 2011). The remaining thin layer is often observed in the present study. In general, this type of dominantly non-refractory particle with no well-defined refractory substance included were the most abundant type of particle in the investigated samples.

In Fig. 5II, an example of a sea salt particle is shown, and there were no significant amounts of non-refractory material associated with that particle. That was the case for several sea-salt particles, but there are also some examples of sea-salt mixed with non-refractory substances. In Fig. 5III.a, an example of a mostly non-refractory particle with a small amount of soot adhering to it (Fig. 5III.b) is shown. These types of particles were typically dominated by the non-refractory material and with only small volume fractions of soot – either adhering to the surface – or covered completely or partly by non-refractory material.

In Fig. 5IV, a soot particle not associated with non-refractory material is shown. Soot particles were by number the most abundant type of refractory substances in the samples studied, however almost all the observed soot particles were internally mixed with

ACPD
15, 30757–30791, 2015

non-refractory matter. In Fig. 5V.a a partly non-refractory particle is shown – as can be seen when comparing to the image in Fig. 5V.b. The refractory part of the particle shown in Fig. 5V.b contained significant amounts of sodium and potassium, and it may originate from biomass burning. In Fig. 5VI a dust particle is shown. In total 4 out of 871 particles were classified as dust in the investigated size range, and they were not or only very slightly associated with non-refractory PM. TEM was also used to study samples in the super-micron range from the same site and aircraft samples collected at different altitudes in the vicinity of Barbados. Mineral dust typically comprised a significant fraction the super-micron particulate matter, and at higher altitudes mineral dust also comprised a significant fraction in the sub-micron size range, which will be described in more detail in future publications.

Five samples from 17–21 June, and three samples from 27 June, and 4 and 11 July were studied (Table 2). The data obtained from the first five samples (period 1) and the last three samples (period 2) respectively, were grouped separately and binned according to the their initial PAED and the volume fraction of any refractory material in the range from 0 to 0.3, from 0.3 to 0.9 and > 0.9 as shown in Fig. 6a and b respectively. The refractory matter was classified as soot, soot mixtures, mineral dust, sea salt and "other", where the last category contains all refractory substances not belonging to any of the first mentioned groups. In Fig. 6a and b, sea-salt is shown separately, while all the other refractory substances are grouped together. In Fig. 6c and d the volume fractions of non-refractory substances and all the different refractory particle groups are shown for period 1 and 2 respectively in different size ranges. It is worth noting that all the volume fractions of refractory PM presented here can be considered upper limits since more volatile species may have evaporated from the studied particles before closer inspection, and in many cases the evaporation of non-refractory PM has already started when the first particle image is produced.

As can be seen from Fig. 6 the majority of the investigated particles belonged to the accumulation mode in the PAED range from 100 to 300 nm. For the first period about 20 % of the 440 studied particles contained well defined refractory material, while it was

ACPD
15, 30757–30791, 2015

about 30 % for the 431 particles in the second group. Out of the particles comprising refractory material – the majority of those were dominated by non-refractory material with a small volume fraction of refractory material. By number the majority of the small refractory particles were classified as soot. Only about 3 and 2 % respectively of all the investigated particles are comprised of a refractory volume fraction larger than 90 % for the two groups of samples. In the PAED range from 100–200 nm, it is only a small fraction (< 10 % by number) of the studied particles that contain any well-defined refractory matter, and in most of those cases the refractory matter comprises a small volume fraction of the particles. For the particles larger than ∼ 300 nm, the refractory matter is relatively more abundant both by number fraction and by volume. In the following section, it will be discussed how the information presented in this section can be combined with results presented in previous sections in order to infer information about the chemical composition of the studied cloud condensation nuclei.

6 Summary and discussion

It has been shown in the sections above that during most of the campaign influences from local land-based particle sources can be expected to be very limited and thus, the investigated aerosol can be considered as representative for the Eastern Caribbean Sea. The CCN number concentrations and total particle number concentration are relatively low – and similar to pristine marine conditions. The particle number size distributions were typically dominated by an accumulation mode with a maximum near ∼ 180 nm. Based on CCN number concentrations and size distributions measured in parallel the critical diameters were inferred and they ranged from ∼ 50 nm for an SS = 0.7 % to ∼ 150 nm for an SS = 0.1 %. The corresponding κ values were typically found in the range 0.2–0.5 for all supersaturations (0.1–0.7 %) with the exception of the first day of measurements, where it is likely that the influence of sea salt was relatively higher. Significant mass concentrations of mineral dust was present during most of the campaign, with occasional high mineral dust mass concentrations. Impactor samples

ACPD
15, 30757–30791, 2015

collected on eight different days, where significant mass concentration of dust was observed, were analysed with TEM. The majority of the investigated particles were found in the accumulation mode, and in general the bulk of the particles were largely dominated by non-refractory substances.

Based on the presented results and some basic assumptions it is possible to estimate to what extent the minor concentration of refractory particulate matter is likely to influence the inferred CCN activity. It can be expected that significant amounts of the non-refractory PM in the studied size range is sulphate species (Li-Jones and Prospero, 1998). Pure ammoniumsulphate and other inorganic sulphate species of atmospheric relevance have κ values of 0.6 or slightly higher when it comes to cloud droplet activation (κ_{CCN}). The κ_{CCN} values inferred in the present study are typically below ~ 0.4. Some basic modeling using Eq. (2) and the information about the refractory PM volume fractions (Fig. 6) in combination with the particle number size distributions (Fig. 2) clearly indicates that the inferred κ values cannot be explained solely by mixtures of sulphate species and the refractory PM even when $\kappa = 0$ is assumed for all the refractory PM. The influence from the refractory PM is negligible since the estimated volume fraction only exceeds 10 % for particles larger then 300 nm, and (i) as can be observed from Fig. 2 only a small number fraction of the CCN are present in that size range, and (ii) most particles (even with low CCN activity) with diameters larger 300 nm will activate into cloud droplets at supersaturations of 0.1 % or higher. Hence, the observed κ values are very likely to reflect a significant organic volume fraction, which is corroborated by the skin-like remainder frequently observed in the TEM evaporation studies.

Most organic species of atmospheric relevance typically have κ_{CCN} values ranging from about ~ 0 up to ~ 0.3 (Petters and Kreidenweis, 2007; Petters et al., 2009). Kristensen et al. (2012) reported average κ_{CCN} values of ~ 0.08 for large fractions of ambient water soluble organic particulate matter in different environments. If such a κ_{CCN} value is assumed for the organic species in the present study, then an internally mixed volume fraction of organic matter at the order of ~ 50 % in the diameter range ~ 50–

ACPD
15, 30757–30791, 2015

200 nm could explain the observations, if it it assumed that the remainder of the PM in that size range is dominated by sulphate species. Such a composition is comparable to what has been reported for particulate matter with diameters below 0.6 µm on Puerto Rico (Novakov et al., 1997). From the TEM studies it seems highly likely that the aerosol particles (at least in the accumulation mode) are internally mixed, but if an external mixture of sulphate and organic species is assumed, then an organic volume fraction at the order of 25 % could also explain the observed κ values.

For the present study, it should be kept in mind that the TEM samples studied are limited with respect to the number or particles investigated and they also represent a limited period of the entire campaign. Nevertheless, (i) a large fraction of the particles investigated with TEM had indications of organic matter as mentioned above, (ii) it is hard to explain ambient κ_{CCN} values in the range from 0.2–0.4 without organic species being present – if refractory matter such as soot and dust is likely to comprise a very minor volume fraction, (iii) significant organic fractions have previously been reported for the size range relevant as CCN in the same region (Novakov et al., 1997; Mayol-Bracero et al., 2001; Maria et al., 2002). So there are several independent observations supporting that organic species are likely to play a role for the CCN activity observed in the present study.

Mineral dust was observed over the Caribbean Sea almost during the entire measurement period and the airmasses generally originated from Northern Africa (Groß et al., 2015), so it cannot be ruled out that organic species in the gas phase or the particle phase also are transported across the North Atlantic. During the summer season significant amounts of biogenic precursers of secondary organic aerosol are emitted in North Western Africa (Capes et al., 2009), which may contribute to secondary organic aerosol in the trade winds. Biomass burning is also a source of organic PM (and soot), but the studied PM was not dominated by biomass burning particles, and biomass burning typically occurs in the dry season during winter in Northern Africa. A study of the organic PM from Puerto Rico in the Eastern Caribbean indicated that oceanic emissions was the dominant source of organic PM Mayol-Bracero et al. (2001). If oceanic

ACPD
15, 30757–30791, 2015

emissions is the main source of the organic PM in the present study, then it can explain the generally low κ values observed, also when the airmasses occasionally may not be influenced from continental sources.

The significant differences in CCN properties observed in the present and previous studies (ranging from very low κ_{CCN} values and dominance by mineral dust to higher κ_{CCN} and dominance of inorganic soluble species) may in part be due to different meteorological conditions and seasonal variations in aerosol particle properties e.g. resulting in high/low biological activity and different vertical atmospheric mixing. It is clear that more and longer term studies will be needed in order to fully assess the CCN properties in the region and to identify the respective roles organic species, nss inorganic species, sea salt and mineral dust.

7 Conclusions

Aerosol particles (with a focus on cloud condensation nuclei properties) were investigated in the trade wind marine boundary layer in the Eastern Caribbean Sea during the SALTRACE campaign, June–July 2013. Local land-based particle sources could be ruled out for almost the entire campaign, and particle number size distributions and concentrations were representative of pristine marine environments. Significant mass concentrations of mineral dust was present during most of the campaign. The inferred CCN activity could be represented by κ values typically in the range from 0.2–0.5 for both the Aitken and the accumulation mode. Investigations of particle compositions with TEM in combination with EDX showed negligible concentrations of mineral dust (< 0.5 % by number), and very minor concentrations of sea salt particles (1–2 % by volume) and soot (∼ 2 % by volume) in the size range of the accumulation mode dominating the CCN number concentrations. The CCN population was almost entirely comprised by non-refractory particulate matter, and based on previous studies in the region and the inferred κ values, it is highly likely that the CCN largely were comprised of a mixture of sulphate and organic species. An estimate of the organic volume frac-

ACPD
15, 30757–30791, 2015

tion of the CCN would depend on the κ value of the organic species – but an organic volume fraction at the order of 50 % is likely.

Acknowledgements. This study was supported by the European FP7 project: "Impact of biogenic vs. anthropogenic emissions on clouds and climate: towards a holistic understanding" (BACCHUS). T. B. Kristensen gratefully acknowledges funding from the German Federal Ministry of Education and Research (BMBF) project 01LK1222B. K. Kandler and M. Hartmann gratefully acknowledge support from the Deutsche Forschungsgemeinschaft (FOR 1525 INUIT and KA 2280/2).

References

Allan, J. D., Baumgardner, D., Raga, G. B., Mayol-Bracero, O. L., Morales-García, F., García-García, F., Montero-Martínez, G., Borrmann, S., Schneider, J., Mertes, S., Walter, S., Gysel, M., Dusek, U., Frank, G. P., and Krämer, M.: Clouds and aerosols in Puerto Rico – a new evaluation, Atmos. Chem. Phys., 8, 1293–1309, doi:10.5194/acp-8-1293-2008, 2008. 30760, 30770

Andreae, M. O. and Rosenfeld, D.: Aerosol–cloud–precipitation interactions, Part 1. The nature and sources of cloud-active aerosols, Earth Sci. Rev., 89, 13–41, doi:10.1016/j.earscirev.2008.03.001, 2008. 30758

Bergametti, G. and Forêt, G.: Dust deposition, in: Mineral Dust, Springer, the Netherlands, 179–200, doi:10.1007/978-94-017-8978-3, 2014. 30771

Bony, S. and Dufresne, J.-L.: Marine boundary layer clouds at the heart of tropical cloud feedback uncertainties in climate models, Geophys. Res. Lett., 32, L20806, doi:10.1029/2005GL023851, 2005. 30759

Capes, G., Murphy, J. G., Reeves, C. E., McQuaid, J. B., Hamilton, J. F., Hopkins, J. R., Crosier, J., Williams, P. I., and Coe, H.: Secondary organic aerosol from biogenic VOCs over West Africa during AMMA, Atmos. Chem. Phys., 9, 3841–3850, doi:10.5194/acp-9-3841-2009, 2009. 30776

Cini, R., Loglio, G., and Ficalbi, A.: Temperature dependence of the surface tension of water by the equilibrium ring method, J. Colloid Interf. Sci., 41, 287–297, 1972. 30765

ACPD
15, 30757–30791, 2015

Garimella, S., Huang, Y.-W., Seewald, J. S., and Cziczo, D. J.: Cloud condensation nucleus activity comparison of dry- and wet-generated mineral dust aerosol: the significance of soluble material, Atmos. Chem. Phys., 14, 6003–6019, doi:10.5194/acp-14-6003-2014, 2014. 30759

Good, N., Topping, D. O., Allan, J. D., Flynn, M., Fuentes, E., Irwin, M., Williams, P. I., Coe, H., and McFiggans, G.: Consistency between parameterisations of aerosol hygroscopicity and CCN activity during the RHaMBLe discovery cruise, Atmos. Chem. Phys., 10, 3189–3203, doi:10.5194/acp-10-3189-2010, 2010. 30769

Groß, S., Freudenthaler, V., Schepanski, K., Toledano, C., Schäfler, A., Ansmann, A., and Weinzierl, B.: Optical properties of long-range transported Saharan dust over Barbados as measured by dual-wavelength depolarization Raman lidar measurements, Atmos. Chem. Phys., 15, 11067–11080, doi:10.5194/acp-15-11067-2015, 2015. 30762, 30776

Heintzenberg, J., Birmili, W., Wiedensohler, A., Nowak, A., and Tuch, T.: Structure, variability and persistence of the submicrometre marine aerosol, Tellus B, 56, 357–367, 2004. 30768

Hudson, J. G.: Variability of the relationship between particle size and cloud-nucleating ability, Geophys. Res. Lett., 34, L08801, doi:10.1029/2006GL028850, 2007. 30770

IPCC: Climate Change: The Assessment Reports of the Intergovernmental Panel on Climate Change, Cambridge University Press, Cambridge, UK, 2013. 30759

Jefferson, A.: Empirical estimates of CCN from aerosol optical properties at four remote sites, Atmos. Chem. Phys., 10, 6855–6861, doi:10.5194/acp-10-6855-2010, 2010. 30769

Jung, E., Albrecht, B., Prospero, J. M., Jonsson, H. H., and Kreidenweis, S. M.: Vertical structure of aerosols, temperature, and moisture associated with an intense African dust event observed over the eastern Caribbean, J. Geophys. Res.-Atmos., 118, 4623–4643, 2013. 30759, 30771

Jurányi, Z., Gysel, M., Weingartner, E., DeCarlo, P. F., Kammermann, L., and Baltensperger, U.: Measured and modelled cloud condensation nuclei number concentration at the high alpine site Jungfraujoch, Atmos. Chem. Phys., 10, 7891–7906, doi:10.5194/acp-10-7891-2010, 2010. 30764

Kandler, K., Benker, N., Bundke, U., Cuevas, E., Ebert, M., Knippertz, P., Rodríguez, S., Schütz, L., and Weinbruch, S.: Chemical composition and complex refractive index of Saharan mineral dust at Izaña, Tenerife (Spain) derived by electron microscopy, Atmos. Environ., 41, 8058–8074, 2007. 30763

Kandler, K., Lieke, K., Benker, N., Emmel, C., Küpper, M., Müller-Ebert, D., Ebert, M., Scheuvens, D., Schladitz, A., Schütz, L., and Weinbruch, S.: Electron microscopy of par-

ACPD
15, 30757–30791, 2015

ticles collected at Praia, Cape Verde, during the Saharan mineral dust experiment: particle chemistry, shape, mixing state and complex refractive index, Tellus B, 63, 475–496, 2011. 30766, 30772

Kiyoura, R. and Urano, K.: Mechanism, kinetics, and equilibrium of thermal decomposition of ammonium sulfate, Ind. Eng. Chem. Proc. DD., 9, 489–494, doi:10.1021/i260036a001, 1970. 30766

Kristensen, T. B., Wex, H., Nekat, B., Nøjgaard, J. K., van Pinxteren, D., Lowenthal, D. H., Mazzoleni, L. R., Dieckmann, K., Koch, C. B., Mentel, T. F., Herrmann, H., Hallar, A. G., Stratmann, F., and Bilde, M.: Hygroscopic growth and CCN activity of HULIS from different environments, J. Geophys. Res.-Atmos, 117, D22203, doi:10.1029/2012JD018249, 2012. 30775

Lide, D. R.: CRC Handbook of Chemistry and Physics, CRC Press/Taylor and Francis, Boca Raton, FL, USA, 2692, 2009. 30766

Li-Jones, X. and Prospero, J. M.: Variations in the size distribution of non-sea-salt sulfate aerosol in the marine boundary layer at Barbados: impact of african dust, J. Geophys. Res.-Atmos., 103, 16073–16084, 1998. 30760, 30775

Maria, S. F., Russell, L. M., Turpin, B. J., and Porcja, R. J.: FTIR measurements of functional groups and organic mass in aerosol samples over the Caribbean, Atmos. Environ., 36, 5185–5196, 2002. 30760, 30776

Mayol-Bracero, O., Rosario, O., Corrigan, C., Morales, R., Torres, I., and Perez, V.: Chemical characterization of submicron organic aerosols in the tropical trade winds of the Caribbean using gas chromatography/mass spectrometry, Atmos. Environ., 35, 1735–1745, 2001. 30760, 30776

Mochida, M., Nishita-Hara, C., Furutani, H., Miyazaki, Y., Jung, J., Kawamura, K., and Uematsu, M.: Hygroscopicity and cloud condensation nucleus activity of marine aerosol particles over the western North Pacific, J. Geophys. Res.-Atmos., 116, D06204, doi:10.1029/2010JD014759, 2011. 30769

Monahan, E. C. and Muircheartaigh, I.: Optimal power-law description of oceanic whitecap coverage dependence on wind speed, J. Phys. Oceanogr., 10, 2094–2099, 1980. 30770

Novakov, T. and Penner, J. E.: Large contribution of organic aerosols to cloud-condensation-nuclei concentrations, Nature, 365, 823–826, doi:10.1038/365823a0, 1993. 30760

ACPD
15, 30757–30791, 2015

Novakov, T., Corrigan, C., Penner, J., Chuang, C., Rosario, O., and Bracero, O.: Organic aerosols in the Caribbean trade winds: a natural source?, J. Geophys. Res.-Atmos., 102, 21307–21313, 1997. 30760, 30776
O'Dowd, C. D. and de Leeuw, G.: Marine aerosol production, Phil. T. Roy. Soc., 365, 1753–1774, 2007. 30769, 30770
O'Dowd, C. D., Facchini, M. C., Cavalli, F., Ceburnis, D., Mircea, M., Decesari, S., Fuzzi, S., Yoon, Y. J., and Putaud, J.-P.: Biogenically driven organic contribution to marine aerosol, Nature, 431, 676–680, 2004. 30759
Petters, M. D. and Kreidenweis, S. M.: A single parameter representation of hygroscopic growth and cloud condensation nucleus activity, Atmos. Chem. Phys., 7, 1961–1971, doi:10.5194/acp-7-1961-2007, 2007. 30759, 30761, 30765, 30770, 30775
Petters, M. D., Kreidenweis, S. M., Prenni, A. J., Sullivan, R. C., Carrico, C. M., Koehler, K. A., and Ziemann, P. J.: Role of molecular size in cloud droplet activation, Geophys. Res. Lett., 36, L22801, doi:10.1029/2009GL040131, 2009. 30770, 30775
Pierce, J. R. and Adams, P. J.: Global evaluation of CCN formation by direct emission of sea salt and growth of ultrafine sea salt, J. Geophys. Res.-Atmos., 111, D06203, doi:10.1029/2005JD006186, 2006. 30759
Pringle, K. J., Tost, H., Pozzer, A., Pöschl, U., and Lelieveld, J.: Global distribution of the effective aerosol hygroscopicity parameter for CCN activation, Atmos. Chem. Phys., 10, 5241–5255, doi:10.5194/acp-10-5241-2010, 2010. 30770
Prospero, J. M. and Lamb, P. J.: African droughts and dust transport to the Caribbean: climate change implications, Science, 302, 1024–1027, 2003. 30759, 30762, 30771
Prospero, J. M., Blades, E., Mathison, G., and Naidu, R.: Interhemispheric transport of viable fungi and bacteria from Africa to the Caribbean with soil dust, Aerobiologia, 21, 1–19, 2005. 30763
Rasband, W. S.: ImageJ, 1.47c, http://rsb.info.nih.gov/ij/, US National Institutes of Health, Bethesda, MD, USA, 2015. 30767
Reade, L., Jennings, S., and McSweeney, G.: Cloud condensation nuclei measurements at Mace Head, Ireland, over the period 1994–2002, Atmos. Res., 82, 610–621, 2006. 30769
Roberts, G. and Nenes, A.: A continuous-flow longitudinal thermalgradient CCN chamber for atmospheric measurements, Aerosol Sci. Tech., 39, 206–221, 2005. 30763
Rose, D., Gunthe, S. S., Mikhailov, E., Frank, G. P., Dusek, U., Andreae, M. O., and Pöschl, U.: Calibration and measurement uncertainties of a continuous-flow cloud condensation nuclei

ACPD
15, 30757–30791, 2015

counter (DMT-CCNC): CCN activation of ammonium sulfate and sodium chloride aerosol particles in theory and experiment, Atmos. Chem. Phys., 8, 1153–1179, doi:10.5194/acp-8-1153-2008, 2008. 30765

Savoie, D. L. and Prospero, J. M.: Aerosol concentration statistics for the northern tropical Atlantic, J. Geophys. Res., 82, 5954–5964, 1977. 30771

Savoie, D. L., Prospero, J. M., and Nees, R. T.: Frequency distribution of dust concentration in Barbados as a function of averaging time, Atmos. Environ., 21, 1659–1663, 1987. 30771

Savoie, D. L., Prospero, J. M., and Saltzman, E. S.: Non-sea-salt sulfate and nitrate in trade wind aerosols at Barbados: evidence for long-range transport, J. Geophys. Res.-Atmos., 94, 5069–5080, 1989. 30759, 30760, 30770

Savoie, D. L., Arimoto, R., Keene, W. C., Prospero, J. M., Duce, R. A., and Galloway, J. N.: Marine biogenic and anthropogenic contributions to non-sea-salt sulfate in the marine boundary layer over the North Atlantic Ocean, J. Geophys. Res.-Atmos., 107, 4356, doi:10.1029/2001JD000970, 2002. 30759, 30760

Sorooshian, A., Padró, L. T., Nenes, A., Feingold, G., McComiskey, A., Hersey, S. P., Gates, H., Jonsson, H. H., Miller, S. D., Stephens, G. L., Flagan, R. C., and Seinfeld, J. H.: On the link between ocean biota emissions, aerosol, and maritime clouds: airborne, ground, and satellite measurements off the coast of California, Global Biogeochem. Cy., 23, GB4007, doi:10.1029/2009GB003464, 2009. 30769

Trapp, J. M., Millero, F. J., and Prospero, J. M.: Temporal variability of the elemental composition of African dust measured in trade wind aerosols at Barbados and Miami, Mar. Chem., 120, 71–82, 2010. 30763

Twohy, C. H., Kreidenweis, S. M., Eidhammer, T., Browell, E. V., Heymsfield, A. J., Bansemer, A. R., Anderson, B. E., Chen, G., Ismail, S., DeMott, P. J., and Van Den Heever, S. C.: Saharan dust particles nucleate droplets in eastern Atlantic clouds, Geophys. Res. Lett., 36, L01807, doi:10.1029/2008GL035846, 2009. 30759

Werner, F., Ditas, F., Siebert, H., Simmel, M., Wehner, B., Pilewskie, P., Schmeissner, T., Shaw, R., Hartmann, S., Wex, H., Roberts, G., and Wendisch, M.: Twomey effect observed from collocated microphysical and remote sensing measurements over shallow cumulus, J. Geophys. Res.-Atmos., 119, 1534–1545, 2014. 30760

Wiedensohler, A., Birmili, W., Nowak, A., Sonntag, A., Weinhold, K., Merkel, M., Wehner, B., Tuch, T., Pfeifer, S., Fiebig, M., Fjäraa, A. M., Asmi, E., Sellegri, K., Depuy, R., Venzac, H., Villani, P., Laj, P., Aalto, P., Ogren, J. A., Swietlicki, E., Williams, P., Roldin, P.,

ACPD
15, 30757–30791, 2015

Quincey, P., Hüglin, C., Fierz-Schmidhauser, R., Gysel, M., Weingartner, E., Riccobono, F., Santos, S., Grüning, C., Faloon, K., Beddows, D., Harrison, R., Monahan, C., Jennings, S. G., O'Dowd, C. D., Marinoni, A., Horn, H.-G., Keck, L., Jiang, J., Scheckman, J., McMurry, P. H., Deng, Z., Zhao, C. S., Moerman, M., Henzing, B., de Leeuw, G., Löschau, G., and Bastian, S.: Mobility particle size spectrometers: harmonization of technical standards and data structure to facilitate high quality long-term observations of atmospheric particle number size distributions, Atmos. Meas. Tech., 5, 657–685, doi:10.5194/amt-5-657-2012, 2012. 30762, 30766

ACPD
15, 30757–30791, 2015

Table 1. The median CCN number concentrations, the median critical diameters (D_c), the average random error on D_c (δD_c), κ values, standard deviations of the κ values (σ_κ), and average random errors on the κ values ($\delta\kappa$) for the different supersaturations.

SS [%]	CCN [cm^{-3}]	D_c [nm]	δD_c [nm]	κ	σ_κ	$\delta\kappa$
0.1	112	159	5	0.32	0.14	0.04
0.2	173	103	4	0.30	0.18	0.05
0.3	195[a]	79[a]	4	0.29[a]	0.13[a]	0.05
0.4	205	64	3	0.31	0.19	0.05
0.7	236	45	2	0.30	0.21	0.06

[a]The CCN counter was only operated with a supersaturation of 0.3 % during the last 15 days of the campaign.

ACPD
15, 30757–30791, 2015

Table 2. Information about the samples investigated with transmission electron microscopy. Date and UTC time represent the beginning of the sampling, while time in DOY is the midpoint of the sampling time. Duration gives the sampling time in minutes. N_p is the number of particles investigated.

date	UTC time [h:min]	time [DOY]	duration [min]	N_p
17.06	15:00	168.63	20	160
18.06	14:03	169.59	12	46
19.06	13:20	170.56	20	29
20.06	13:50	171.58	20	57
21.06	18:20	172.77	20	148
period 1 in total			92	440
27.06	02:45	178.13	30	169
04.07	13:50	185.59	30	148
11.07	13:07	192.55	18	114
period 2 in total			78	431

ACPD
15, 30757–30791, 2015

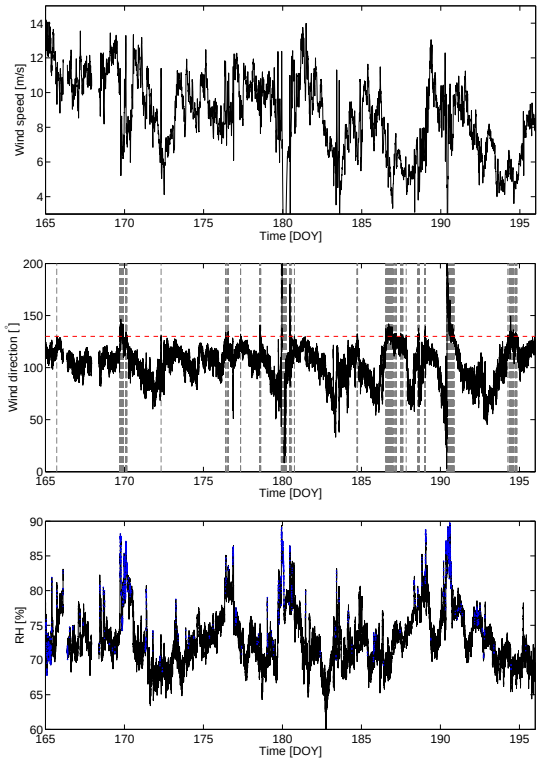

Figure 1. Local meteorological parameters measured at the top of the 17 m high tower. Top panel: the wind speed. Mid panel: the wind direction. The grey dashed vertical lines indicate time periods where influence from local sources cannot be ruled out (wind directions in the range from 130 to 335°). Lower panel: the measured relative humidity with blue points indicating time periods with rain.

ACPD
15, 30757–30791, 2015

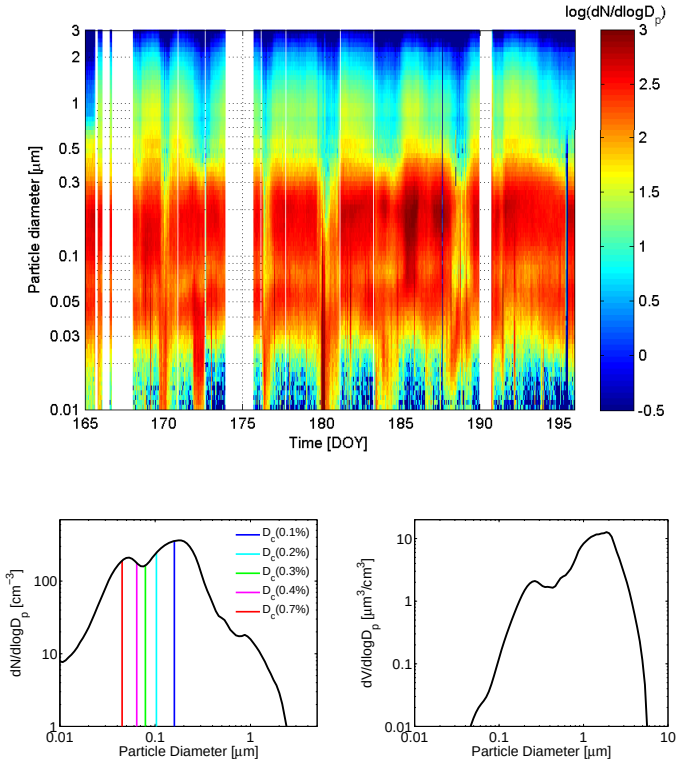

Figure 2. Size distributions not corrected for particle losses in the tubing nor corrected for detection efficiency. MPSS data covers the mobility diameter range 0.01–0.8 µm, and APS data covers the range for volume equivalent diameters above 0.8 µm. Top panel: the measured aerosol particle number size distributions vs. time in days of year. The colour scale indicates the 10-based logarithm of dN/dlog(D_p) in cm^{-3}. Lower panel: the median particle number size distribution, and the inferred median particle volume size distribution assuming spherical particles. The inferred median critical mobility diameters (D_c) are indicated with vertical lines for the different supersaturations together with the particle number size distribution.

ACPD
15, 30757–30791, 2015

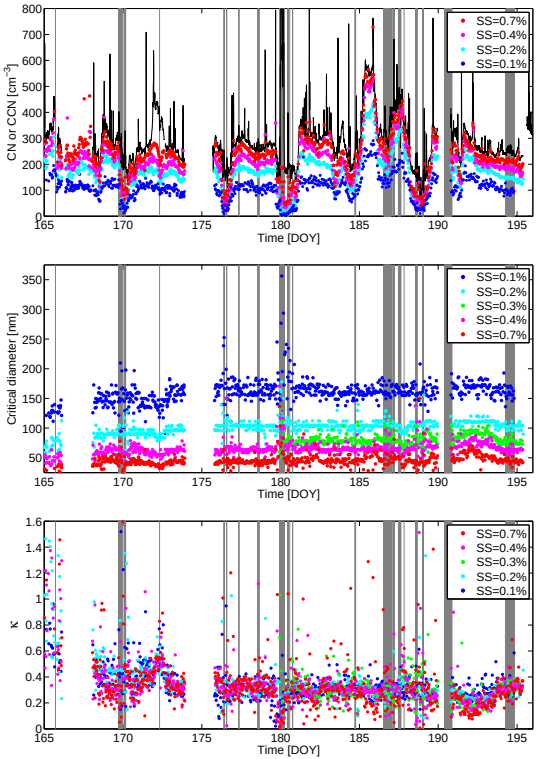

Figure 3. The measured CCN concentrations and associated properties. The grey shaded areas indicate time periods where local land based contamination cannot be ruled out as determined from the local wind direction. Top panel: the measured CCN number concentrations for the different supersaturations. The total particle number concentration (CN) inferred from the MPSS measurements is indicated with the full black line. Mid panel: the inferred critical diameter. Lower panel: the inferred κ values.

ACPD
15, 30757–30791, 2015

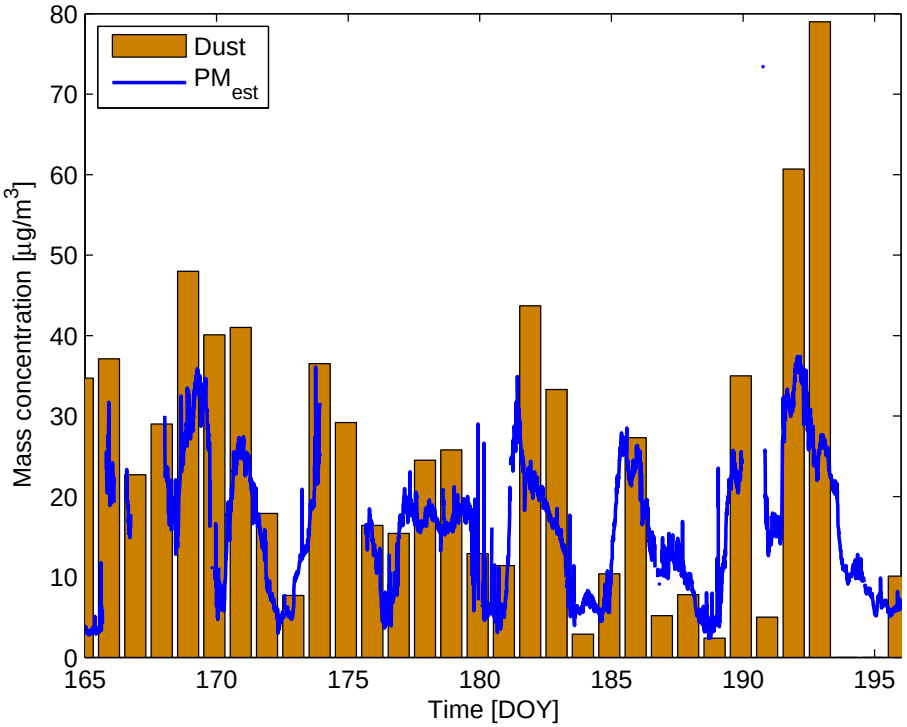

Figure 4. The mineral dust mass concentration (bars) and the particulate matter concentration (PM_{est}, blue line) estimated from the integrated particle volume size distribution for diameters larger than 0.5 µm assuming spherical particles and a particle density of 2.6 g cm^{-3}. The gap in the dust concentration around DOY = 194–195 is due to lack of data for those two days.

ACPD
15, 30757–30791, 2015

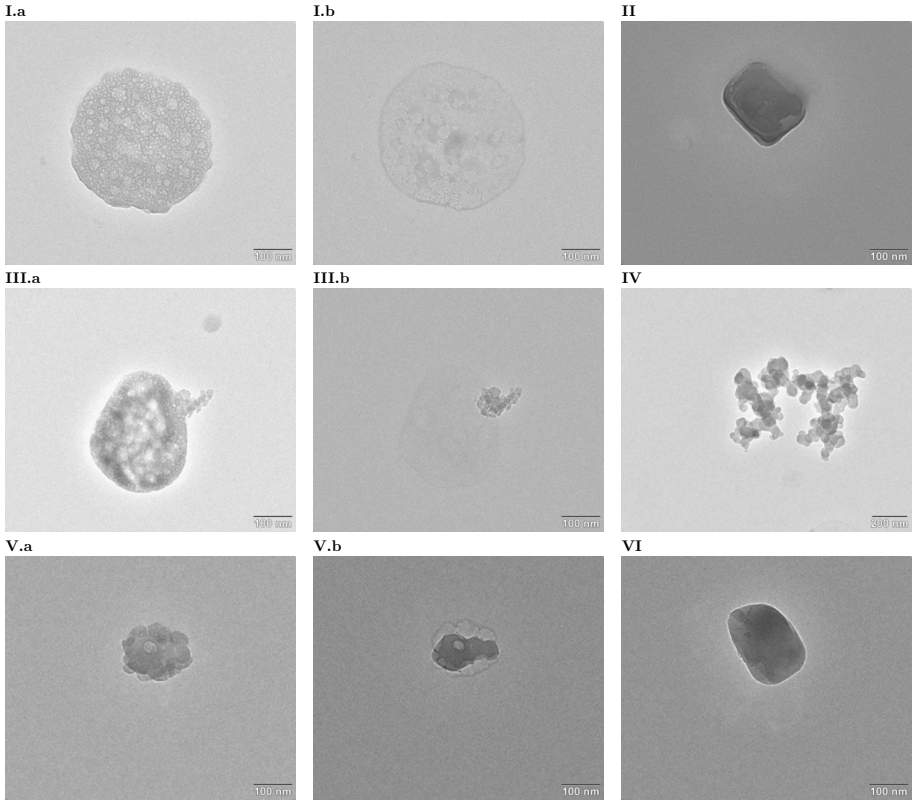

Figure 5. Transmission electron microscope bright field images of collected aerosol particles. Images I.a+b, III.a+b, and V.a+b are before and after evaporation of non-refractory material respectively. For II, IV, and VI no significant evaporation was observed. I: an example of a non-refractory particle. II: sea salt particle. III: A non-refractory particle with a small soot particle adhering to the surface. IV: A soot particle. V: Refractory particle with significant amounts of sodium and potassium. VI: A dust particle. The bar in the lower right corner of each image represents 100 nm, with the exception of IV, where it represents 200 nm.

ACPD
15, 30757–30791, 2015

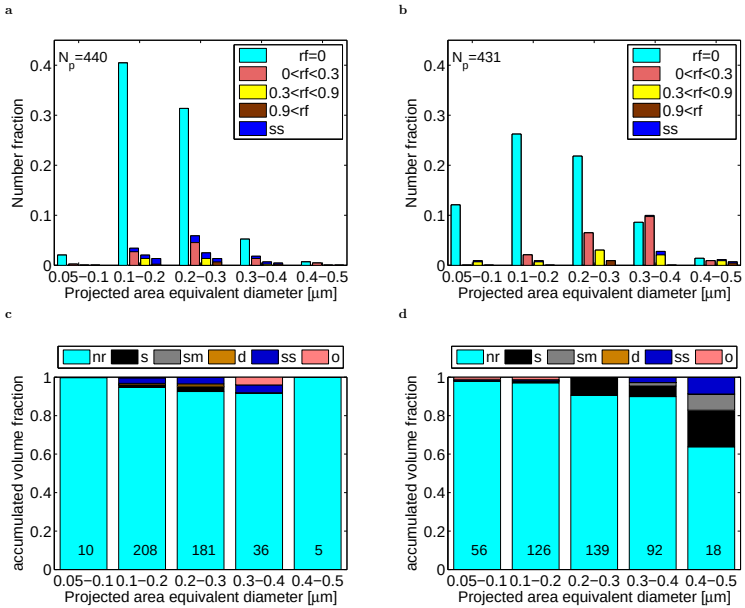

Figure 6. The classification of particles analysed with transmission electron microscopy. In **(a)** and **(b)** representing two different periods of the campaign: the fraction of the total number of particles studied (N_p) grouped according to the initial projected-area-equivalent diameter and the estimated refractory volume fraction (rf) from left to right: with no refractory substances (cyan), with volume fractions of refractory substances in the range up to 0.3 (indianred), in the range from 0.3 to 0.9 (yellow), and in the range higher than 0.9 (brown), with sea-salt (ss) excluded. Sea-salt is shown separately in blue in all the volume fraction ranges. In **(c)** and **(d)**, the volume fractions of the different groups of substances are shown: non-refractory (nr), soot (s), soot-mixtures (sm), dust (d), sea-salt (ss) and the refractory substances not falling into any of these classes are classified as "other" (o) for the same time periods as in **(a)** and **(b)** respectively. The numbers included in the lower part of each bar are the total number of particles with an initial PAED in that size range. More details about the individual samples are given in Table 2.

ACPD
15, 30757–30791, 2015